Available online at www.sciencedirect.com
SCIENCE DIRECT®
European Polymer Journal 40 (2004) 549–560
EUROPEAN POLYMER JOURNAL
www.elsevier.com/locate/europolj

Elastic modulus profiles in the cross sections of drying alkyd coating films: modelling and experiments

Giuseppe Mirone [a], Beáta Marton [b,*], G. Julius Vancso [b,*]

[a] Department of Industrial and Mechanical Engineering, University of Catania, Viale Andrea Doria 6, 95125 Catania, Italy
[b] Faculty of Science and Technology and Dutch Polymer Institute, University of Twente, P.O. Box 217, 7500 AE Enschede, The Netherlands

Received 20 June 2003; received in revised form 24 October 2003; accepted 24 October 2003

Abstract

The temporal development of the modulus of elasticity and its profile were studied in water-borne alkyd coatings during the drying process of the coating films. Values of the Young's moduli of elasticity of free coating films were measured using tensile tests. Since the elastic modulus is related to cross-link density, the values of the moduli give information on the advancement of the drying process. A mathematical model was developed to predict the degree of effective cross-linking and the mechanical behaviour of the drying coating films with different thicknesses. This model is based on trends observed by confocal Raman microspectroscopy, which exhibit the profile of the consumption of double bonds and thus can be used to monitor the development of cross-link density as a function of depth from the film surface. The average values of the Young's measured moduli were successfully described by the numerical model as a function of drying time.

Keywords: Alkyds; Drying; Confocal Raman microspectroscopy; Tensile; Modulus

1. Introduction

The use of water-borne paints is swiftly growing because of increasing awareness regarding harmful health and environmental aspects inherent to organic solvents in solvent-borne systems [1]. As a result, in many countries strict legislation has been, or is being, introduced which severely reduces the use of organic solvents.

Alkyd polymer resins consist of oil-modified polyesters obtained by condensation polymerization of polyhydric alcohols and polyhydric acids, and fatty acids (see Fig. 1) [2,3]. Alkyd resins have been transferred into water-borne coatings by emulsification processes using surfactants [4]. Nowadays alkyd water-borne coatings, compared to solvent-borne alkyds, show excellent performance in many areas, but there is still a lack of understanding of many relevant details of the drying process.

The drying process can be divided into two main steps. First the water should evaporate (physical drying). In the second step chemical "drying" takes place, a part of which is related to chemical network formation [5]. The basic process in the hardening of alkyd paints is the auto-oxidation of the unsaturated fatty acid chains and cross-linking between the chains. Various reaction strategies for chemical cross-linking of alkyds have been reviewed elsewhere [6,7]. One of the possible routes is displayed in Fig. 2. The cross-linking process transforms the coating from an initially incoherent and gel-like state, to a solid layer capable of bearing mechanical load. The network formation starts from the surface and

* Corresponding authors. Tel.: +31-534-893-322; fax: +31-5348-938-23 (B. Marton), tel.: +31-534-892974; fax: +31-53-48-938-23 (G.J. Vansco).
E-mail addresses: b.marton@ct.utwente.nl (B. Marton), g.j.vancso@ct.utwente.nl (G.J. Vancso).

0014-3057/$ - see front matter © 2003 Elsevier Ltd. All rights reserved.
doi:10.1016/j.eurpolymj.2003.10.017

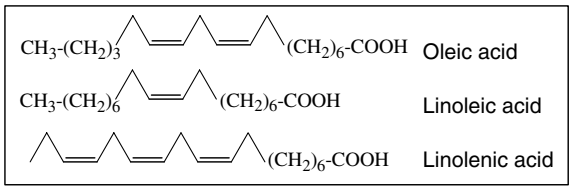

Fig. 1. Typical fatty acids for alkyds [3].

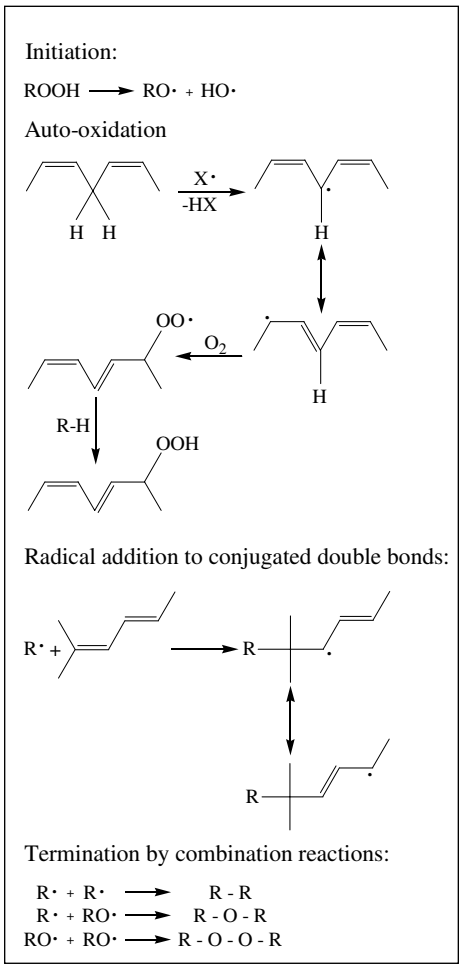

Fig. 2. Scheme for the oxidative drying of oils [6,7].

proceeds toward the inner zones of the coating layer. In order for cross-linking to proceed, a certain amount of oxygen must pass through the already reticulated outer part, which is less permeable to oxygen, to reach the film interior. During cross-linking, with increasing cross-link density the molecular and segment mobility decrease, thus the value of the glass transition temperature, T_g increases. This limits the oxygen penetration through the already dried layer [8]. As a result of the diffusion penetration of oxygen, the alkyd film is drying heterogeneously. Such heterogeneous network formation of alkyd coatings leads to inferior properties during the initial state of drying.

From these considerations it is obvious that there is a need for detailed knowledge of the cross-linking process in the depth of the coating film. Measurements aiming at studies of the temporal network development can be divided into two groups. One possible approach is aiming at measuring chemical changes, the other focuses on the determination of mechanical properties related to cross-link density in the alkyd coatings during the film formation process. There are several studies describing the development of mechanical properties during curing [9–11]. Some common approaches include cross-sectioning of a given layer and direct analysis of the material which can be done using various techniques [12]. However the oxidative alkyd coatings containing drier are very reactive in the presence of oxygen. If a fresh free surface is exposed to oxygen, the oxidation of fatty acid chains starts immediately, which limits the easy applicability of such cross-sectioning approaches.

Since the cross-linking process cannot be prevented in the presence of oxygen, the characterization of the film formation process requires a non-invasive in situ technique. Magnetic resonance imaging (MRI) has been established as a valuable non-invasive tool in material science [13,14]. Hyper frequency scanning acoustic microscopy is an alternate non-destructive microprobing technique [15]. Raman spectroscopy has also been used to investigate the chemical cross-linking mechanism of alkyd coatings in bulk films [16,17]. This latter spectroscopic technique can be also used in a confocal arrangement which enables the optical sectioning of films using an adjustable pinhole able to block any light from outside the focal plane. The confocal aperture is designed to collect the Raman scattering only from a distinct laser focal volume [18]. This technique can potentially measure the onset of cross-linking spatially resolved in the depth of the alkyd films [19,20]. During cross-linking the double bond concentration decreases and finally approaches zero. Monitoring the change of C=C double bonds in the coating layer as a function of depth from the surface gives information on the progress of the drying process. Confocal Raman microspectroscopy (CRM) offers a unique possibility to examine this problem. In this work we use it to determine how the extent and rate of cross-linking varies as a function of depth in an alkyd coating. To demonstrate the time dependence of double bond consumption by oxidative cross-linking as a function of depth, representative data by CRM are shown. This allows us to gain insight into the dependence of oxygen penetration inhibition as a function of depth and distance from the sample surface.

The use of tensile modulus measurements to follow the cross-linking is based on the rubber elasticity theory

[21]. The elastic modulus of an elastic network is proportional to the cross-link density described as:

$$E = 3vRT_a \quad (1)$$

where v is the effective concentration of elastically active cross-linked chains in moles per gram (including both physical and chemical cross-links), R is the gas constant, and T_a is the absolute temperature. As with the progress of the cross-linking, the value of the Young's modulus increases, its value can be used as an indicator for the advancement of the drying process [22,23]. During oxidative network formation, the value of the elastic modulus of the coating increases from an almost zero value to a saturation value, which is typical for the completely dried coating film. In the same time, the viscous modulus of the resin decreases progressively until a stable value is approached when drying is complete.

One of the most widely used methods to obtain E values is the mechanical tensile test, where a free film is strained at a constant rate until it breaks. This standard technique has been frequently used for coatings [24].

The present work is focused on building a mathematical model to describe changes of the bulk elastic modulus during the drying process as a function of drying time and film thickness. The model used applies a profile based on experimental data measured by CRM, and tensile tests, and uses some assumptions. The model can also predict the percentage of cross-linking accomplished and calculate the local Young's modulus of the corresponding, partially dried coating layers after different ageing times and for different values of film thickness. Modelling of the modulus as a function of drying time, film thickness and depth in the film has been defined in a phenomenological way and verified experimentally in this work.

2. Experimental section

2.1. Materials and sample preparation

The coating studied was a commercial alkyd emulsion paint. The alkyd emulsion was made from an alkyd resin based on soya-bean fatty acids with an oil length of 40% and acid value 10 mg KOH/g alkyd. The commercial short oil alkyd emulsion (URADIL AZ554 Z-50) was supplied by the DSM Coating Resins, Zwolle. It is an alkyd typically used as a binder for solvent-borne alkyd paints applied in decorative and maintenance sectors. The term oil length denotes the fatty acid content relative to the solvent-free resin [25,26]. A water emulsifiable cobalt drier was used to catalyze the chemical oxidation of the fatty acid components.

For the confocal Raman measurements, alkyd emulsion films with a thickness of 150 μm were cast on glass slides. The resulting coating films were dried under normal laboratory conditions. After the evaporation of the water from the coating, the film thickness was approximately 70 μm.

Dog-bone shaped tensile specimens were prepared for mechanical measurements by pouring different amounts (ranging from 1.5 to 6 ml) of the emulsion coating into an appropriate silicone cast to obtain samples with predetermined thickness. These films were also dried under normal laboratory conditions. The nominal gauge length and width of the specimens were 34 and 5.5 mm respectively. The thicknesses assigned to each series, (ranging from 0.5 to 1.9 mm after 3 days ageing, and from 0.2 to 1.2 mm after 30 days ageing) [1], correspond to the values on the date of the experiments to consider and minimize the influence of thickener and shrinkage during drying.

2.2. Techniques

Confocal Raman microscopy was used to measure the double bond concentration decrease during the chemical cross-linking process [17]. Raman spectra were measured of the alkyd films by a custom-made confocal Raman microspectrometer using a 25 μm confocal pinhole [18]. A Kr ion-laser (Coherent, Innova 90-K) provided the excitation wavelength of 647.1 nm. A dry 63X objective (Zeiss Plan Neofluar) with a numerical aperture (NA) of 0.85 was used for the acquisition of all Raman spectra. The spectra were recorded with 30 mW laser power and accumulation times of 30 s were employed. The depth profiling experiment was started by taking a spectrum at the surface of the film, followed by collecting spectra at steps of four micrometers in depth until the glass substrate was reached. In order to determine the degree of cure from a Raman spectrum, the strength of the C=C bond absorption at 1655 cm^{-1} (Fig. 3) must be monitored relative to another peak, at 1000 cm^{-1}, that is unaffected by curing.

Mechanical tensile experiments were performed using an Imada tensile testing machine, composed of a DPX-T dynamometer (maximum load 500 Newton) and a LV-100 bench. The specimens were tested at different elongation levels. A digital micrometer recorded the displacements with an accuracy of 10 μm. For each test, the machine crosshead was manually translated to a desired position. Subsequently, six load measurements were taken at time intervals of 30 s. The corresponding

[1] These film thicknesses are high comparing with the real applied coating film thicknesses, however they enable the measurements and we suppose that the results are also applicable for thinner films.

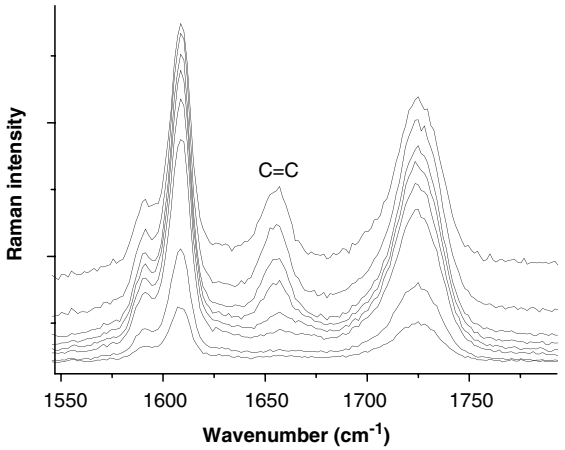

Fig. 3. Typical Raman spectra exhibiting the depth dependence of the C=C absorption due to inhomogeneous double bond concentration in alkyd resins. The individual spectra from the bottom to the top represent optical sections as a function of increasing depth from the surface.

load value decrease was measured until 180 s of elapsed time. This procedure was repeated until a total of six elongation levels were imposed and the corresponding load values were taken for each specimen tested.

3. Results and discussion

3.1. Confocal Raman microspectroscopy

The CRM measurements reveal the decay of double bond concentration as a function of film nominal depth after different drying times (Fig. 4). Nominal depth is defined as the distance between the preset focal point and the film surface. In practice we collect spectra of focal volumes which are placed deeper in the film than the nominal depth [27,28]. The depth resolution problem for alkyd films is discussed in another paper [19]. Double bond concentration decrease is related to the onset of the oxidative cross-linking process. Thus, the decrease in the double bond concentration provides information regarding the advance of the cross-linking process. The extent of cross-linking is not homogenous in depth, as can be observed from the measured profiles (see in Fig. 3). The cross-linking proceeded from the surface (in direct contact with air) in the direction of the substrate.

A typical "drying front" profile can be observed in Fig. 4 which is moving with increasing drying time in the direction of the deeper layers of the film. This front suggests the influence of a limiting factor in the cross-linking process, which is presumed to be related to the presence of oxygen. The inflection points of typical fractions of C=C bond profiles in the measured curves

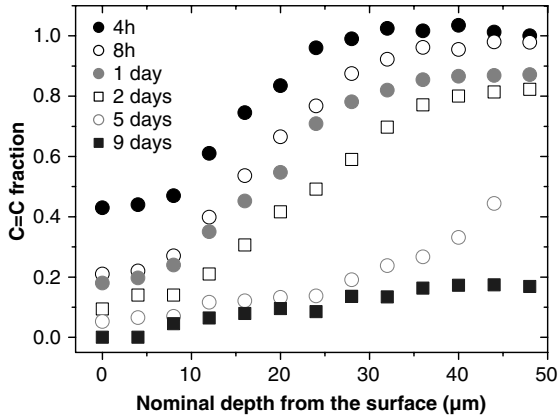

Fig. 4. Decay of double bond fraction as a function of nominal depth from the free surface of the coating films after different drying times.

provide information on the progress of cross-linking. The curves can be divided into three regions: there are two plateau levels and there is a transition region. Close to the sample surface, to a depth of 10 μm, there is no significant difference in C=C concentration as a function of film depth. This means that there is no oxygen penetration limitation for these film thicknesses, as the drying is homogenous in this range.

3.2. Tensile tests

Tensile tests were performed on a series of specimens at various ageing times (from 3 to 35 days at room temperature). In order to reduce the influence of the viscous component of the mechanical response, typical for viscoelastic (polymeric) binders, the corresponding stress value for each strain was measured over 180 s after the application of the strain for different ageing times and specimen thickness values. Fig. 5 shows the viscoelastic behavior of the coatings in terms of the decrease in load at different imposed elongations, within a time range of 180 s. For every measurement, the time of 180 s assures an acceptable load stabilization. The load relaxation is faster after longer drying times, and for thinner films, respectively.

The length of the specimens after the unloading process, measured after a recovery time of 1 day, resulted in values almost identical to those of the undeformed state, indicating the absence of plastic deformation. The load relaxation data from Fig. 5 can also be plotted as load–elongation curves (Fig. 6). Such graphs characterize the decrease of actual axial stiffness of the coating in the first seconds after removal of the loading until stabilization occurs within 180 s (where the viscous component of the response is negligible). The difference in the slopes of load–extension curves at

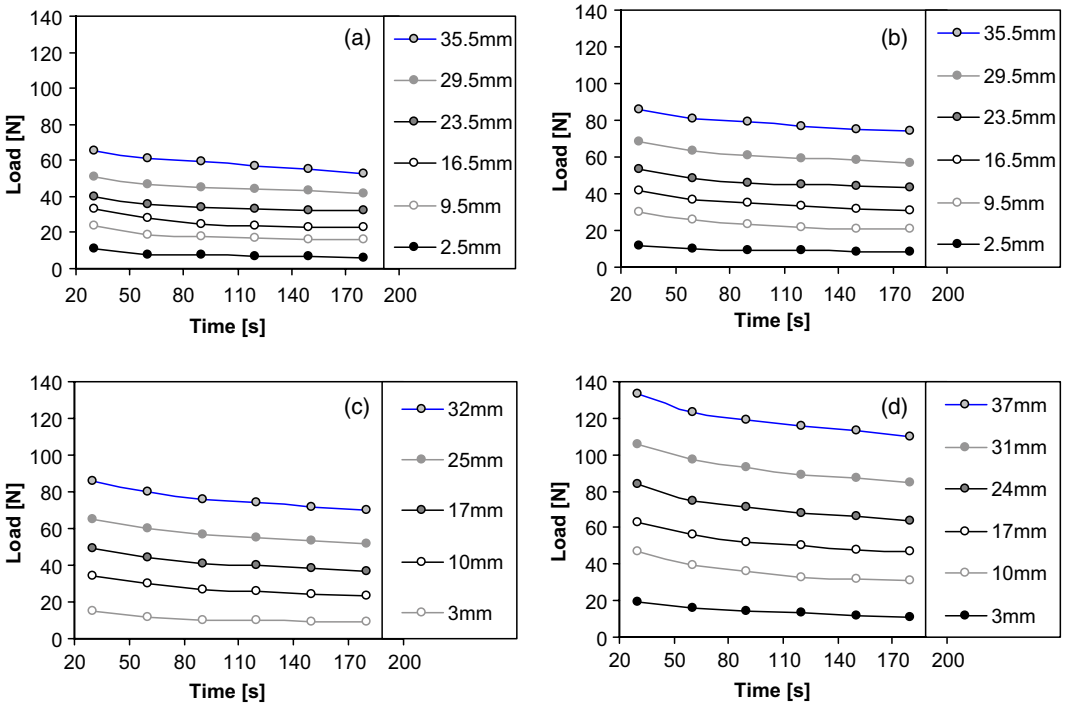

Fig. 5. Load relaxation experiments at different elongation levels. Measurements were made on films of different thickensses, T and ageing time, t: (a) $T = 0.4$ mm and $t = 15$ days; (b) $T = 1$ mm, $t = 15$ days; (c) $T = 0.4$ mm, $t = 35$ days; (d) $T = 35$ mm, $t = 35$ days.

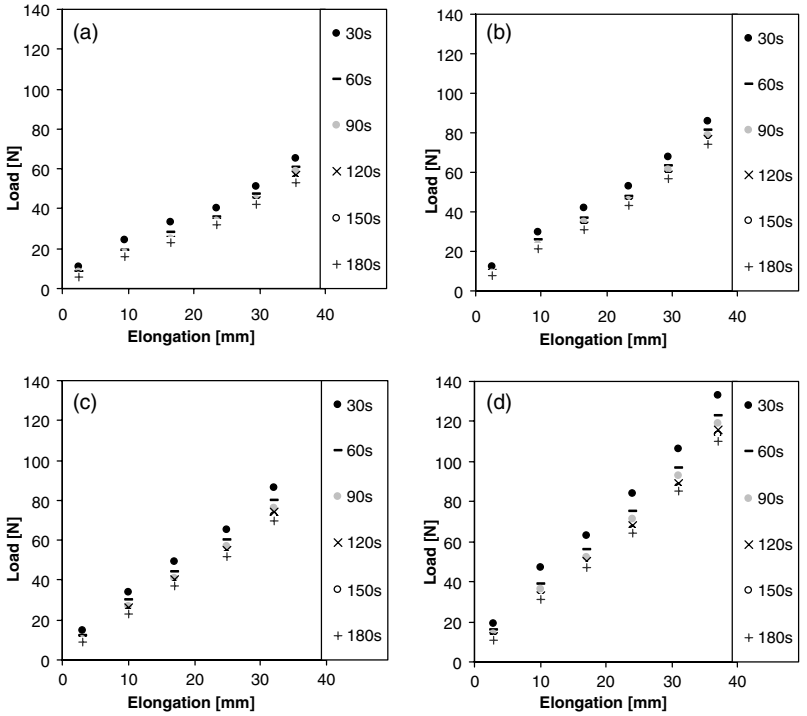

Fig. 6. Load–elongation curves obtained at 30–180 s relaxation times for different thicknesses, T and ageing times, t: (a) $T = 0.4$ mm and $t = 15$ days; (b) $T = 1$ mm, $t = 15$ days; (c) $T = 0.4$ mm, $t = 35$ days; (d) $T = 1$ mm, $t = 35$ days.

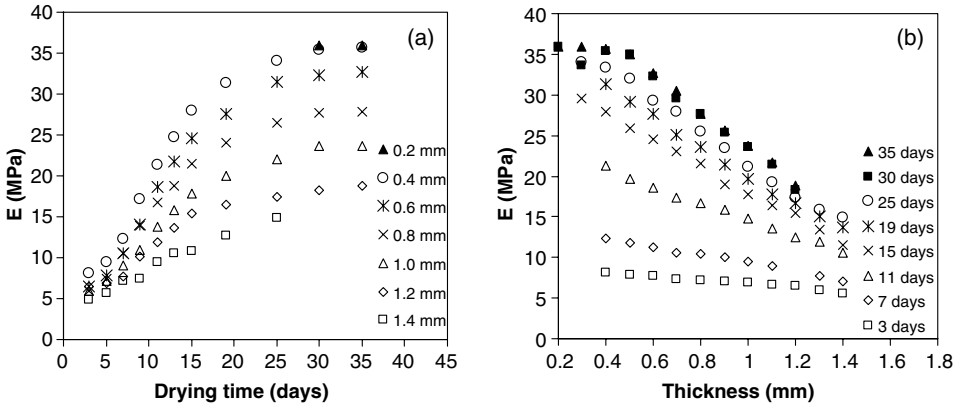

Fig. 7. Experimental elastic modulus values (a) versus drying time, for different thickness values, as parameters and (b) versus film thickness, for different drying times, as parameters.

different relaxation times indicates that also the macroscopic modulus $E_{\text{bulk}}(t,T)$ exhibits variations due to viscoelastic effects in the first 180 s after straining.

The previously mentioned bulk modulus $E_{\text{bulk}}(t,T)$ (as a function of ageing time, t and film thickness, T), is obtained from the curves of Fig. 6 by simply dividing the stress (applied force per unit cross section area) by the strain (elongation normalized on the initial specimen length) [29]. For the model calculations, to be described later, the stabilized load value measured 180 s after the application of the strain was used. Obviously, the average value of the modulus, $E_{\text{bulk}}(t,T)$ is the result of the contributions from all infinitesimal layers in the cross-section of the film, each layer having its local value of the modulus $E(t,T)$ as a function of depth, z, from the central plain of the film. The bulk modulus is the sum of the values of the moduli of the layers of different cross-link densities. The calculations we describe are based on simple equations for predicting the modulus of composite materials [30,31].

The calculated E_{bulk} values are shown in Fig. 7 as a function of the increasing ageing time (with overall film thickness as parameter) and as a function of the thickness (with ageing time as parameter), respectively. The trends show that the maximum value of the elastic modulus $E_{\max}$ is approximately 36 MPa.

It is clear from Fig. 7 that the value of the bulk elastic modulus of the coating gradually increases during the drying process until a plateau value is reached. The plateau value of the modulus is the same for films with thicknesses smaller than ±0.4 mm. However, above this value of thickness, the plateau value decreases with increasing coating thickness, as can be seen in the experimental results discussed above. This clearly indicates the presence of a threshold thickness, beyond which complete cross-linking of the inner layers is impossible. After a certain elapsed time of oxidative cross-linking, the surface of the coating is completely reticulated, becoming difficult for oxygen to penetrate and virtually preventing oxygen to reach the mean-plane zone (still incompletely cross-linked). Since the uncrosslinked core of the film has a lower E, and this core becomes larger with thicker films, the plateau E will be a function of the film thickness if the overall thickness is beyond a given characteristic value (on our experimental time scale of drying).

4. A composite model describing the elastic modulus during film drying

In order to model the mechanical properties (modulus) of coatings with heterogeneous modulus profiles, a function e, ranging from zero to one, is introduced to express the fraction of complete cross-linking at each depth level across the thickness of the coating. In case of the uncrosslinked coating, $e = 0$ and for a completely cross-linked material, $e = 1$. This function depends on the ageing time, t, on the considered depth, z, and on the coating thickness, T (Fig. 8), i.e. $e = f(t,T,z)$.

To derive the relationship expressing $e(t,T,z)$, at a given time t prior to the complete cross-linking of the entire coating, the function e (Fig. 9) should decrease continuously from the exposed surface ($z = \pm T/2$), which is assumed to be completely dried within ca. one day, toward the central plane of the film ($z = 0$). If both external surfaces of the coating are exposed to air (free film), the function e has a minimum value due to the symmetry at $z = 0$. If the coating is cast on an entirely airtight surface, the situation is conceptually the same (due to symmetry) but the z origin must be placed on the cast-coating interface (where the contact with air is minimum) instead of the mean plane.

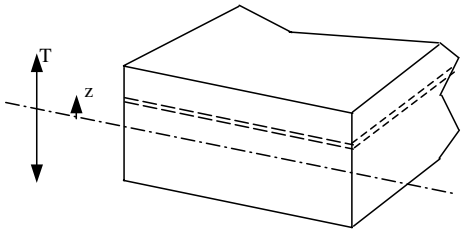

Fig. 8. Thickness and level (depth) definition in the drying film.

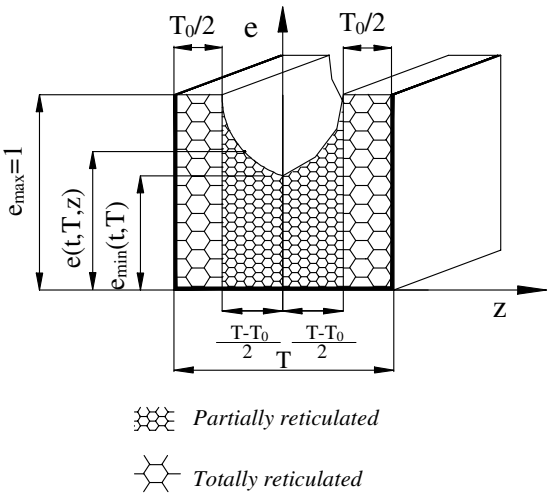

Fig. 9. Distribution of the cross-linking variable along the thickness for a free film.

As a first hypothesis, the dependence between e and z is estimated to be parabolic as roughly indicated by CRM (Fig. 4). We assume that the double bond concentration decrease is directly related to the advancement of cross-linking. The parameters of the parabola in the middle section of the film depend on the ageing time t and on the total thickness T. With these assumptions, the distributions of the cross-linking function e along the thickness, at different ageing times, have the shapes qualitatively drawn in Fig. 10.

At a time t, only the T_0 portion of the entire thickness is completely cross-linked. The value of T_0 increases during the drying until it becomes equal to the thickness T, i.e. until the entire coating film is completely dried. As previously mentioned, the experiments showed that if T was larger than a certain value (about 0.4 mm), then the elastic modulus did not reach the maximum value typical for the thinner films during the timescale of the drying experiment. This suggests that in case of large thicknesses, the complete network formation of the inner layers is significantly retarded, thus T_0 does not become equal to the total thickness (again, during the timesale of observations) and the coating remains only partially dried (Fig. 11).

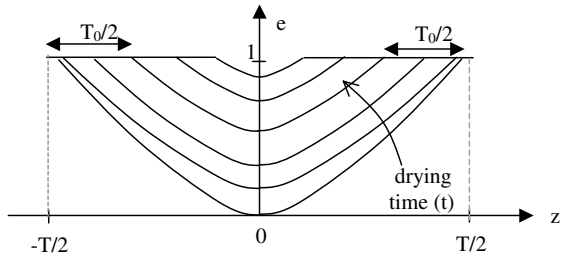

Fig. 10. Distribution of the cross-linking variable at different drying stages.

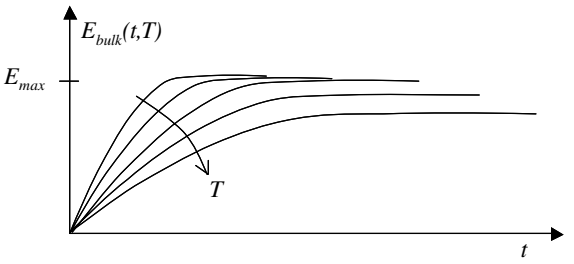

Fig. 11. Elastic modulus increase (average over the entire cross-section of the film) during network formation.

The parabolic relationship between e and z is described by Eq. (2),

$$e(t,T,z) = e_{\min}(t,T) + e_1(t,T)\cdot z^2 \tag{2}$$

where $e_{\min}$ is a specific minimum value of the drying indicator at a time, t and for a film with a thickness, T (Fig. 9), while e_1 is the coefficient determining the parabola curvature.

As a second hypothesis, we assume that the local value of the Young's modulus, E depends linearly on the cross-linking parameter, e, as expressed by Eq. (3)

$$E(t,T,z) = E_0 + (E_{\max} - E_0)\cdot e(t,T,z) \tag{3}$$

E_0 represents the elastic modulus of the totally uncross-linked coating, and $E_{\max}$ is the modulus value at complete network formation. In our case E_0 can be set to zero because the coating at $t = 0$ is a liquid-like material. The measurement was carried out at low deformation rates (infinitely long times) when liquids have a almost zero modulus, thus Eq. (3) becomes:

$$E(t,T,z) = E_{\max}\cdot e(t,T,z) \tag{4}$$

Eq. (4) shows that $E_{\max}$ plays the role of a scale factor, thus the distribution of the elastic modulus has the same shape of that representing the cross-linking index and can be schematically represented analogously to Fig. 10 at a given time, t and thickness, T. In other words, the $e(t,T,z)$ function may also be seen as the elastic modulus normalized by its maximum value $E_{\max}$.

A combination of Eqs. (2) and (4) yields the expression for the local elastic modulus:

$$E(t,T,z) = E_{\max} \cdot \lfloor e_{\min}(t,T) + e_1(t,T) \cdot z^2 \rfloor \tag{5}$$

The parabolic distributions described by Eqs. (2) and (5), obviously apply only for $|z| < (T - T_0)/2$, where the coating film is partially dried. In the zones where the coating drying is completed, the modulus is uniformly distributed, similar to the cross-linking function (Figs. 4 and 5), and their values are $E_{\max}$ and *1*, respectively. $E_{\max}$ can be obtained from tensile tests performed on the specimens $(T < T_{\text{th}})$ after full cross-linking is approached (long drying times). In order to calculate the complete distributions of the elastic modulus and the cross-linking parameter along the coating thickness, two unknown parameters ($e_{\min}$ and e_1) remain to be determined for each set of t and T.

To determine the values of the parameters $e_{\min}$ and e_1 in Eq. (5), the following conditions were imposed:

(1) Boundary condition: the modulus reaches its maximum possible value $E_{\max}$, corresponding to the completely dried material, for $|z| = (T - T_0)/2$, at a given time t;
(2) Equilibrium condition: the sum of the applied stresses for each cross section equilibrates the overall total stress. Thus, the average modulus over the entire thickness is equal to the bulk modulus of the whole specimen $E_{\text{bulk}}(t,T)$ determined from experimental macroscopic tensile tests on partially dried coating films. This condition follows from the theory for composite materials made of layers with different elastic properties [30,31].

In order to apply these conditions in the form of mathematical constraints for Eq. (5), the function $T_0(t)$ must be known. This function, specific for the given coating used, can be obtained by fitting the experimental data presented in Fig. 7. The determination of $T_0(t)$ will be discussed later. The typical experimental $E_{\text{bulk}}(t)$ curves at different thickness values are similar to those schematically shown in Fig. 11. From these trends it is possible to determine the correspondence between the completely dried thickness fraction $T_0(t)$ and drying time, and it is also possible to determine the threshold thickness T_{th}, for which the complete network formation cannot be reached. In fact, T_{th} can be detected as the parameter of the first curve for which the plateau value is lower than $E_{\max}$. Clearly, for completely dried films with $T < T_{\text{th}}$, the macroscopic modulus corresponds to the local value of $E_{\max}$ uniformly distributed along the thickness.

Assuming that the functions of $T_0(t)$, $E_{\text{bulk}}(t,T)$ and the values of $E_{\max}$ are known, condition 1 can be expressed as:

$$E\left(t,T,\frac{T-T_0(t)}{2}\right) = E_{\max}\left[e_{\min}(t,T) + e_1(t,T)\cdot\left[\frac{T-T_0(t)}{2}\right]^2\right] = E_{\max} \tag{6a}$$

Condition 2 can be expressed as:

$$\frac{1}{T}\left\{E_{\max}\cdot T_0(t) + \int_{-\frac{T-T_0(t)}{2}}^{\frac{T-T_0(t)}{2}} E_{\max}\left[e_{\min}(t,T) + e_1(t,T)\cdot z^2\right]\cdot \mathrm{d}z\right\} = E_{\text{bulk}}(t,T) \tag{6b}$$

Eq. (6a) can be rewritten as:

$$e_1(t,T) = [1 - e_{\min}(t,T)]\cdot\frac{4}{[T-T_0(t)]^2} \tag{7}$$

which allows us to determine the function $e_1(t,T)$.

Substituting $e_1(t,T)$ from Eq. (7) into Eq. (6b) results in the following equation:

$$\frac{E_{\max}}{T}\left\{T_0(t) + \int_{-\frac{T-T_0(t)}{2}}^{\frac{T-T_0(t)}{2}}\left[e_{\min}(t,T) + [1-e_{\min}(t,T)]\cdot\frac{4}{[T-T_0(t)]^2}\cdot z^2\right]\cdot \mathrm{d}z\right\} = E_{\text{bulk}}(t,T) \tag{8}$$

This equation cannot be easily solved analytically because the interval of integration is a function of time (t). Numerical solutions, for an adequate number of ageing times (t), thickness values (T) and bulk moduli (E_{bulk}) (all values experimentally measurable), give parameter sets $[t, T, e_{\min}]$ from which with fitting, it is possible to obtain the $e_{\min}(t,T)$ function. Once this function is derived and introduced in Eq. (7), Eq. (5) gives the local distributions of E, which are otherwise not measurable.

For thickness values lower than T_{th}, the time interval at which the increasing E_{bulk} reached the value of $E_{\max}$, information about the relationship $T_0(t)$ could be gathered. From the above data, values of t *and* T_0 were determined and successively approximated by the fourth order polynomial $T_0(t)$ (Eq. (8)) plotted in Fig. 12 together with the experimental points. The following numerical values were used for fitting in Fig. 12:

$$T_0(t) = 1.87\times10^{-2}\times t - 5.98\times10^{-4}\times t^2 + 2.11\times10^{-5}\times t^3 - 3.051\times10^{-7}\times t^4 \tag{9}$$

The plot in Fig. 12 suggests that the threshold thickness has a value close to 0.4 mm. As indicated earlier, for this threshold thickness complete drying is obtained after a period of 35 days.

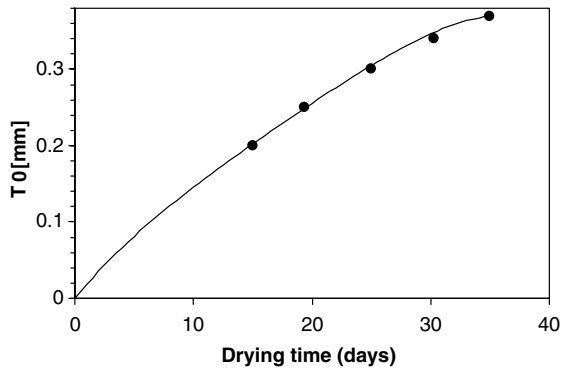

Fig. 12. Fitting law of the dried thickness $T_0(t)$ for a particular film.

Since $T_0(t)$ and $E_{\max}$ are known, Eq. (8) can be solved for given thickness values and ageing times, in order to obtain data sets for $(t, T, E_{\min})$, where $E_{\min} = E_{\max} e_{\min}$ is the minimum value of $E(t, T, z)$. These data sets were fitted with the following quadratic law in the particular case studied here:

$$E_{\min}(t,T) = E_{\max}\left[0.1313 + 0.0356 \times t + 0.000177 \times t^2 - 0.4584 \times T + 0.3174 \times T^2 - 0.03389 \times t \times T\right] \quad (10)$$

Finally, we would like to summarize the steps of the modelling procedure described by the flow chart shown in Fig. 13.

5. Numerical approximations and comparison with the experimental results

Eqs. (9) and (10), together with the values found for $E_{\max}$, allow one to predict the values of the elastic modulus E and of the cross-linking function e along the thickness of the coating, for every ageing time and thickness combination. Fig. 14 shows the result for two films with different thickness. Two predictions resulting from the model are reported in Fig. 14, in terms of elastic modulus distribution along the thickness (or accomplished drying percentage distribution, dividing the modulus by $E_{\max}$) for two different thickness values. The different curves of the charts represent different ageing times. Proceeding from the lower to the higher

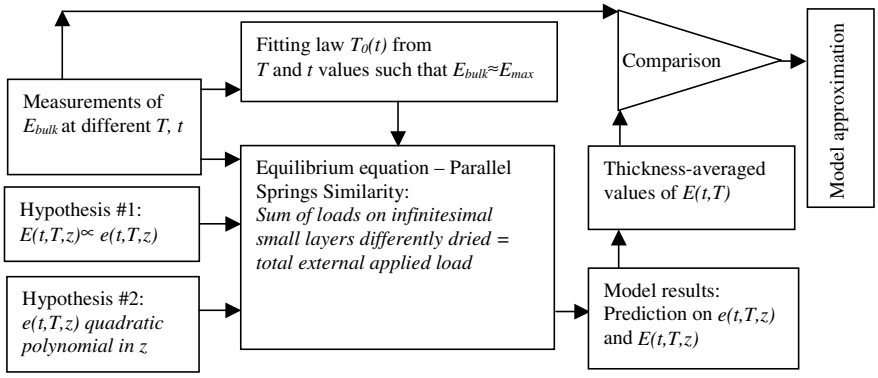

Fig. 13. Flow chart of the modelling procedure.

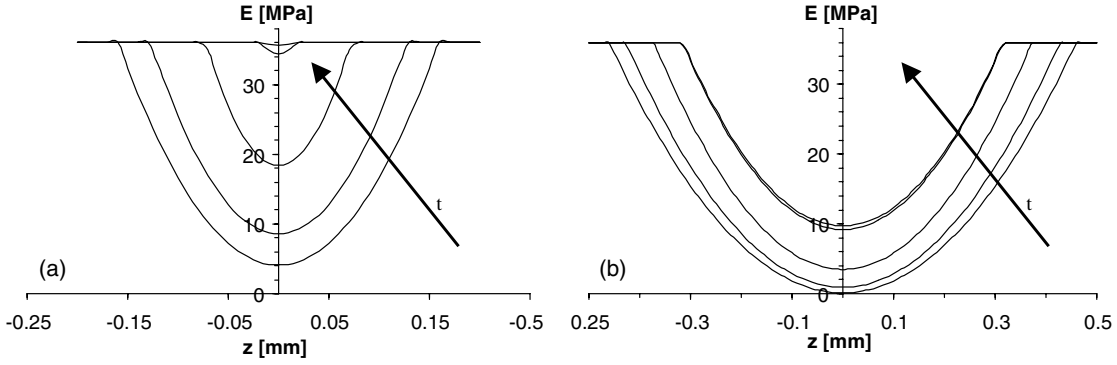

Fig. 14. Elastic modulus distributions along the thickness for (a) 0.4 and (b) 1 mm thick coatings after 5, 10, 20, 35 and 60 days of drying, respectively.

curves, we are referring to times varying from the early to the final stages of the drying process.

The prediction for the increase of the modulus in the core of the coating, shown in Fig. 14, is in qualitative agreement with the trends of the experimental values of E_{bulk} presented in Fig. 7. As an example, for specimens dried longer than 20 days, the modulus at the center of the film (0.4 mm) reaches 3/5 of the maximum value, but in the core of the 1 mm thick film the modulus is almost zero. Fig. 14 shows an almost complete drying in the case of thin samples (0.4 mm thick specimen is dried for about 90% of its thickness after 35 days), and a large extent of incomplete drying for thicker films (only about 40% for the 1 mm thick coating after 35 days).

In Fig. 15 the predictions from the model for the elastic modulus increase are shown during a 60 days time interval at three height levels: midplane ($z \approx 0$), immediate proximity of the exposed surface ($z = T/2$) and halfway between these two locations ($z = T/4$), for the same thickness values examined in the previous figures. It is also visible that for the inner layer of the coating the stiffness is predicted to grow later and to become constant at a lower value for the thicker coatings as compared with the thin ones. In the thicker coating, the $T/4$ plane cannot solidify completely, i.e. it remains at a cross-linking stage of about 66% corresponding to an elastic modulus of 24 MPa.

Finally in Figs. 16 and 17 the comparisons between the macroscopic modulus estimations from the model and the corresponding experimental measurements are displayed. Integrating Eq. (4) across the thickness of the coating allows us to evaluate the average modulus. The simulation and the experimental results are in reasonable agreement, especially for longer ageing times. For shorter drying times the model is less reliable as in such cases the films have inferior integrity with respect to those obtained at sufficiently long drying times. This deviation is likely due to the less accurate thickness measurements and the larger viscous component contributions to the virtual observed E modulus.

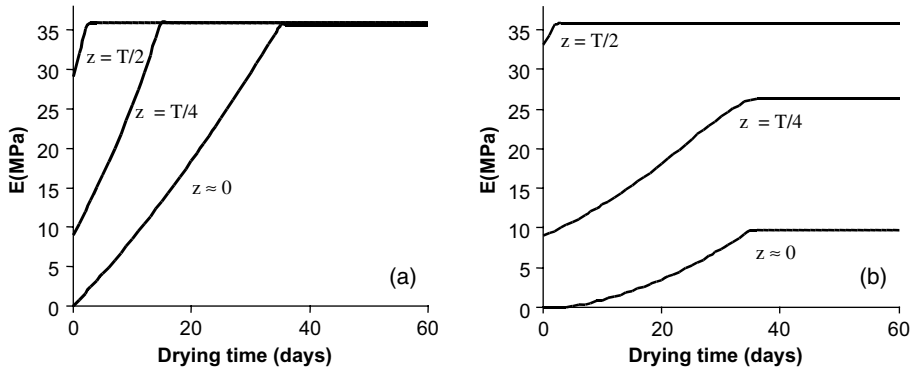

Fig. 15. Modulus development during 60 days of ageing time for (a) 0.4 and (b) 1 mm thick coatings.

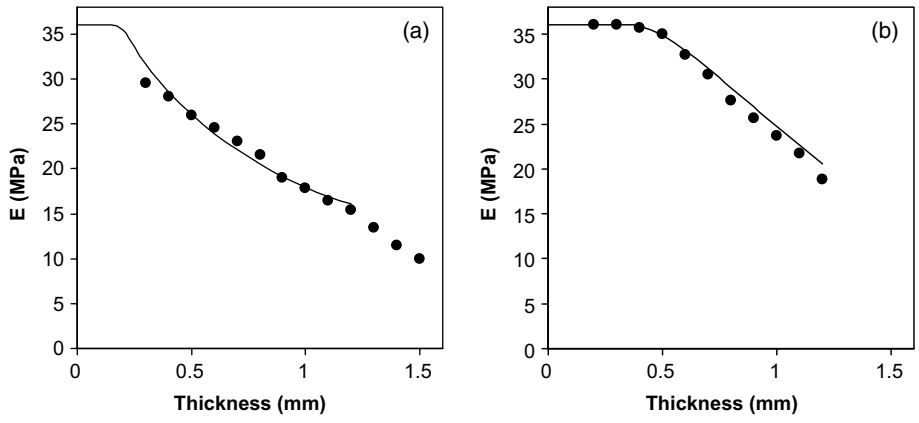

Fig. 16. Experimental and numerical macroscopic moduli versus thickness for a film after (a) 15 days and (b) 35 days of drying time.

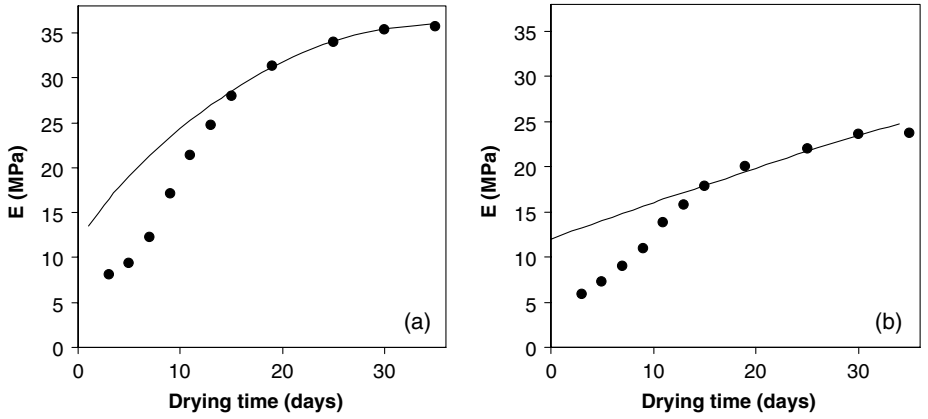

Fig. 17. Experimental and numerical macroscopic moduli versus drying time for a film with (a) $T = 0.4$ mm and (b) $T = 1$ mm thickness.

6. Conclusions

A model has been developed to give information on modulus variation in the depth of the film during the drying process, the completely dried film thickness at a given time and the maximum possible thickness of the completely cross-linked coating film.

The outer layers of the films become completely cross-linked after a very short time compared to the time of complete drying. A threshold thickness was experimentally determined, beyond which complete network formation becomes practically impossible (on the time scales of this study). Two assumptions were made, the first includes the elastic response as proportional to the accomplished drying fraction; the second assumes that the modulus shows a parabolic distribution with the distance from the midplane for the partially dried coating at room temperature. The second assumption was supported by confocal Raman microscopy results. From these assumptions a set of polynomial relationships were derived whose parameters were evaluated from the fitting of a reduced set of experimental data. This allowed a reasonable reproduction of the drying–stiffening behavior of the coating observed experimentally.

The proposed characterization methodology, applied to a suitable number of materials of the same family, could lead to a database of industrial interest in all those cases where detailed time–mechanical property relationships are needed.

Acknowledgements

The authors thank Mr. Leo van der Ven (Akzo Nobel Coatings Research Arnhem) for the very useful and stimulating discussions. The authors gratefully acknowledge the financial support by the Priority Program Materials (PPM) of NWO-CW and the Dutch Polymer Institute (DPI). DSM Resins is acknowledged for providing the alkyd emulsion samples.

References

[1] de Hek H, Zabel KH, Geurink PJA. Surf Coat Aust 1998;35:14–22.
[2] Edwards J. Coating and surface treatment systems for metals: a comprehensive guide to selection. Stevenage: Finishing; 1997.
[3] Lanson HJ. Alkyd resins. In: Mark HF, Bikales NM, Overberger CG, Menges G, editors. Encyclopedia of polymer science and engineering. New York: John Wiley & Sons; 1985. p. 644–79.
[4] Weissenborn PK, Motiejauskaite A. J Coat Technol 2000; 72:65–74.
[5] Hofland A. Making paint from alkyd emulsions. In: Glass JE, editor. Technology for waterborne coatings, ACS Symposium Series 663. Washington: American Chemical Society; 1997. p. 183–95.
[6] Muizebelt WJ, Donkerbroek JJ, Nielen MWF, Hussen JB, Biemond MEF. J Coat Technol 1998;70:83–93.
[7] Swern DJ, Coleman JE, Knight HB, Ricciuti C, Willits CO, Eddy CR. J Am Chem Soc 1953;75:3135–7.
[8] Zetterlund PB, Johnson AF. Polymer 2002;43:2039–48.
[9] Gillham JK. Polym Int 1997;44:262–76.
[10] Provder T. J Coat Technol 1989;61:32–50.
[11] Palmese GR, Gillham JK. J Appl Polym Sci 1987;34:1925–39.
[12] Adamsons K. Prog Polym Sci 2000;25:1363–409.
[13] Glover PM, McDonald PJ, Newling B. J Magn Res 1997;126:207–12.
[14] Wallin M, Glover PM, Hellgren A-C, Keddie JL, McDonald PJ. Macromolecules 2000;33:8443–52.
[15] Comte C, von Stebut J. Surf Coat Technol 2002;154:42–8.
[16] Claybourn M, Agbenyega JK, Hendra PJ, Ellis G. Adv Chem Ser 1993;236:443–82.

[17] Agbenyega JK, Claybourn M, Ellis G. Spectrochim Acta 1991;47A:1375–88.
[18] Sijtsema NM, Wouters SD, de Grauw CJ, Otto C, Greve J. Appl Spectrosc 1998;52:348–55.
[19] Marton B, van der Ven LGJ, Otto C, Uzunbajakava N, Hempenius MA, Vancso GJ. Polymer (to be submitted).
[20] Marton B, van der Ven LGJ, Otto C, Uzunbajakava N, Hempenius MA, Vancso GJ. Polym Mater: Sci Eng 2003;88:445–6.
[21] Ferry JD. Viscoelastic properties of polymers. New York: John Wiley; 1980.
[22] Hill LW. Prog Org Coat 1997;31:235–343.
[23] Zosel A. Prog Org Coat 1980;8:47–79.
[24] Hill LW. Mechanical properties of coatings. Philadelphia: Federation of Societies for Coatings Technology; 1987.
[25] Wicks ZW. Organic coatings. New York: Wiley-Interscience; 1999.
[26] Turner GPA. Introduction to paint chemistry and principles of paint technology. London: Chapman and Hall; 1990.
[27] Everall NJ. Appl Spectrosc 2000;54:773–82.
[28] Everall NJ. Appl Spectrosc 2000;54:1515–20.
[29] McCrum NG, Buckley CP, Bucknall CB. Principles of polymer engineering. Oxford University Press; 1997.
[30] Hull D, Clyne TW. An introduction to composite materials. Cambridge: Solid State Science Press; 1996.
[31] Bogdanovich AE, Pastore CM. Mechanics of textile and laminated composites. London: Chapman & Hall; 1996.